






ARTICLE

Heteroatom-doped reduced graphene oxide/polyaniline nanocomposites with improved n-type thermoelectric performance

Mariam Kassim Ali^{1,2}  | Amr Hessein^{3,4}  | Mohsen A. Hassan¹  |
Mohsen Ghali⁵  | Nagih M. Shaalan^{6,7} | Koichi Nakamura^{8,9} |
Ahmed Abd El-Moneim^{1,4} 

¹Department of Materials Science and Engineering, Egypt-Japan University of Science and Technology, New Borg El Arab City, Alexandria, Egypt

²Department of Mining, Materials and Petroleum Engineering, Jomo Kenyatta University of Science and Technology, Nairobi, Kenya

³Department of Mathematical and Physical Engineering, Faculty of Engineering (Shoubra), Benha University, Cairo, Egypt

⁴Graphene Center of Excellence for Energy and Electronic Applications, Egypt-Japan University of Science and Technology, New Borg El Arab City, Alexandria, Egypt

⁵School of Basic and Applied Science, Egypt-Japan University of Science and Technology, New Borg El Arab City, Alexandria, Egypt

⁶Physics Department, Faculty of Science, Assiut University, Assiut 71516, Egypt, Egypt

⁷Department of Physics, College of Science, King Faisal University, Al-Ahsa, 31982, Saudi Arabia

⁸Department of Mechanical and Electrical System Engineering, Kyoto University of Advanced Science, Kyoto, Japan

⁹Center for the Promotion of Interdisciplinary Education and Research, Kyoto University, Kyoto, Japan

Correspondence

Mariam Kassim Ali, Department of Materials Science and Engineering, Egypt-Japan University of Science and Technology, New Borg El Arab City, Alexandria 21934, Egypt.
Email: mariamu.kassim@ejust.edu.eg and kassimali05@gmail.com

Funding information

Japan International Corporation Agency; Science and Technology Development Fund, Grant/Award Number: 31306

Abstract

Polyaniline (PANI) is a potential candidate for n-type thermoelectric (TE) materials owing to its intrinsic electrical conductivity, low thermal conductivity, and facile synthesis techniques. However, its low Seebeck coefficient and power factor have limited its widespread usage. In this study, nitrogen-doped, and sulfur-nitrogen co-doped reduced graphene oxide (rGO) were used for tuning the TE properties of PANI. Doped rGO and PANI/doped-rGO nanocomposites were prepared via hydrothermal technique and chemical oxidative polymerization respectively and thereafter characterized. The TE properties of the nanocomposites were also studied and an optimized Seebeck coefficient, power factor and zT value of -1.75 mV K^{-1} , $95 \mu\text{W m}^{-1} \text{ K}^{-2}$ and 0.06, respectively were reported for the PANI nanocomposite containing 1 wt% sulfur-nitrogen co-doped rGO. These results suggest that PANI/heteroatom-doped rGO can serve as promising candidates for n-type based TE applications.

KEYWORDS

energy filtering, heteroatom-doping, polyaniline, reduced graphene oxide, Seebeck coefficient

1 | INTRODUCTION

Global energy demand has necessitated significant effort to be dedicated to finding alternative sources for sustainable energy. Thermoelectricity is one approach that offers a promising route for power generation from the big percentage of waste heat generated from human activities.^{1–3} To achieve widespread use and commercialization of thermoelectric (TE) materials, they must possess a high figure of merit (zT) or power factor (PF) as described in the following Equation (1) below:

$$zT = \frac{\sigma S^2}{\kappa} T = \frac{PF}{\kappa} T \quad (1)$$

where S , T , σ , and κ are the Seebeck coefficient, absolute temperature, electrical, and thermal conductivities, respectively. The state-of-the-art inorganic TE materials like BiTe, BiSb, PbTe, and so forth have shown high PF and zT factors.^{4,5} However, limitations arising from toxic components, rigidity, heaviness, high-cost have prompted the search for alternative organic materials for such thermoelectric applications. Moreover, thermoelectric generators (TEGs) requires a junction comprising of both p-type and n-type thermoelectric materials for proper device fabrication and operation.^{4,5} Unfortunately, the lack of high performing organic n-type TE materials limits the quick advancing of this promising technology.

Polyaniline (PANI) which is a conducting polymer (CP) has lightweight, low toxicity, low production cost, low thermal conductivity coupled with a high intrinsic electrical conductivity and this makes it attractive for TE applications.^{6–8} Its facile synthesis, easy doping/dedoping process and structural diversification has also attracted its adoption for application as an n-type material.^{9,10} Nevertheless, its relatively low Seebeck coefficient, the low electrical conductivity of PANI in the range of 10^{-7} – 3×10^2 S cm⁻¹ has resulted in extremely low PF 10^{-6} – 10^{-10} W m⁻¹ K⁻² hindering the extensive application of PANI in TEG.^{11,12} Graphene-based materials have sparked a special interest in tuning TE properties of PANI owing to its outstanding electronic and mechanical properties.^{13–16} Nonetheless, the zero-band gap of graphene limits its usage in many applications. Heteroatom-doping with single elements such as phosphorous, nitrogen, sulfur, boron and more recently co-doping has been adopted for tailoring the Fermi level and hence the electronic properties of graphene.^{16–18} Previous reports on PANI/graphene-related TE materials have shown enhanced TE properties; however, this came at the expense of large amounts of graphene loading as high as 70 wt%, additionally, most of these materials exhibited p-type behaviors.^{19–24}

Recently, efforts have been devoted to finding polyaniline-based n-type TE materials however, the limited availability of suitable reductants for controlling the charge carrier density for effective transport and other n-type inducing approaches have not been very successful. Consequently, the conductivity of many n-type materials still falls at just over 1 S cm⁻¹ when compared to that of p-type CPs which have exceeded 1000 S cm⁻¹ after doping. Furthermore, concerns related to air and operation stabilities have also been a major concern.²⁵ By functionalizing polyaniline with ionic liquid and thereafter heat treatment, D. Yoo et al., achieved an electrical conductivity, n-type Seebeck coefficient, and PF of 2.3 mS cm⁻¹, -138.8 μ V K⁻¹, and 4.43×10^{-3} μ W m⁻¹ K⁻², respectively.²⁶ C.O. Yoon et al., reported a conductivity of 6.3 S cm⁻¹ and Seebeck coefficient of -3 μ V K⁻¹ at 300 K for their H₂SO₄ doped polyaniline.²⁷ In a study by M. Hua et al., they enhanced the electrical conductivity to 10^{-1} – 10^{-2} S cm⁻¹ by using strong reductants such as KH and NaH.²⁸ In another study, F. Yakuphanoglu and co-workers added up to 8 wt% DWNT to PANI and reported a Seebeck coefficient of -12 μ V K⁻¹ coupled with 11 orders of magnitude increase in their electrical conductivity.²⁹

With the newly emerging concept of ionic Seebeck coefficient which arises from the Soret effect, outstandingly high ionic Seebeck of up to -18 mV K⁻¹ has been achieved.^{30–32} However, the not satisfying ionic conductivity, the high-cost, and the inferior thermal stability issues of the prepared materials still hinder the advancement of such a promising approach. Till now, no study has been dedicated to using the ionic Seebeck technique for boosting the thermoelectric properties of PANI despite its merits. This, therefore, opens a window for exploiting ionic transport mechanism for novel n-type polyaniline-based TE materials. This study will therefore focus on the dual enhancement of TE characteristics of PANI by employing ionic transport characteristics and heteroatom-doped reduced graphene oxide (rGO). To the best of the authors' knowledge, there are no reports dedicated to investigating the synergistic effect of PANI/heteroatom-doped rGO nanocomposites to produce n-type TE material with improved performance.

This study has therefore focused on fabricating and characterizing of heteroatom-doped rGO and using it to improve the TE properties of PANI. The doped rGO will be fabricated via a hydrothermal technique while the nanocomposites will be synthesized by in situ chemical oxidative polymerization of PANI in the presence of the doped rGO. Structural and morphological analysis of the prepared materials will be conducted and finally, the effect of sulfur and nitrogen co-doped rGO (SNrGO) and nitrogen-doped rGO (NrGO) on the TE performances of PANI will be studied and discussed.

2 | EXPERIMENTAL

2.1 | Synthesis of heteroatom-doped reduced graphene oxide

All chemicals were a reagent grade, sourced commercially and used without any further purification. Initially, GO was synthesized using the modified Hummers' method.^{16,33,34} Afterward, a 2 mg ml⁻¹ solution of the as-synthesized GO was prepared by ultrasonically dispersing GO in deionized water for 1 h. Doping of the GO was achieved using urea (nitrogen source) and thiourea (sulfur and nitrogen source) and the weight ratio of the GO/dopant was adjusted to 1:30. The GO/dopant mixture was sonicated for 15 min and the solution transferred to a 50 ml Teflon-lined stainless-steel autoclave and kept at 180 °C for 12 h. The N_rGO and S_{Nr}GO aerogels were collected and washed with copious amounts of water to remove excess ammonia and sulfur related by-products and dried at 60 °C overnight.³⁵

2.2 | Synthesis of PANI and PANI-rGO nanocomposites

The polyaniline nanocomposites were prepared by in situ polymerization according to Gomes et al.,³⁶ however, with slight modifications. A known weight of doped rGO was sonicated in 1 M HCl for 45 min until a homogeneous dispersion of the rGO was obtained as shown in Figure 1. 2 ml of aniline monomer was added and sonicated for another 15 min and the dispersion placed in an ice bath. To this, an aqueous solution of ammonium persulfate previously prepared in 1 M HCl was added and the polymerization reaction left to completion for 24 h. The greenish-black PANI-rGO powder was collected and washed with copious amounts of water, 1 M HCl and ethanol to remove the residual oxidant and oligomers and the product dried overnight at 70 °C. The weight percentage ratio of N_rGO and S_{Nr}GO to aniline monomer used in the polymerization was set at 1 and 5 wt%. Subsequently, the nanocomposite samples were labeled as P_{Nr}GO-1/P_{Nr}GO-5, and P_{SNr}GO-1/P_{SNr}GO-5, respectively. Pristine PANI was synthesized using the above procedure, however, without rGO addition and the sample labeled as PANI-EB. Thermoelectric samples were prepared by cold pressing the powder into pellets by a 60 kN hydraulic press to a thickness of about 3 mm and a diameter of 13 mm.

2.3 | Physicochemical characterizations

Structural analysis was studied using X-ray powder diffractometer (XRD, Shimadzu, XRD-6100) equipped with

Cu K α radiation, Fourier transform infrared spectroscopy (FTIR, Bruker, Vertex 70) and Raman spectroscopy (Renishaw, Bruker). Elemental analysis and chemical environment were analyzed using X-ray photoelectron spectroscopy (XPS, Thermo Fisher Scientific) device equipped with monochromatic X-ray Al K- α . The morphological studies were carried out by transmission electron microscopy (TEM, JEOL JEM-2100F) and scanning electron microscopy (SEM, JEOL JSM-5900) while energy-dispersive spectroscopy (EDX) analysis and mapping were done using SEM equipped with EDX (SEM Quanta FEG 250).

2.4 | Thermoelectric measurements

The thermal conductivity measurement was carried out using the thermal analyzer (Hot Disk TPS 2500 s). A 7577 Kapton coated sensor which simultaneously acts as a heat source and a thermometer was placed between two identical samples. The input power and time were varied accordingly to prevent heat flow to the outer boundaries of the sample. The data was collected and analyzed using the Hot Disk Thermal Analyzer 7.3 software. The DC electrical conductivity was determined by studying the current-voltage characteristics using a two-point probe set-up connected to a Keithley source meter (Model 6221) and a Keithley nano voltmeter (Model 2182A). The electrical resistivity was then calculated according to $\rho = VA/It$, where V is the applied voltage, I the measured current, A is the pellet cross-section area, and t is the pellet thickness, respectively. Seebeck coefficient measurements were performed using a custom-built laboratory set-up which included Keithley nano voltmeter (Model 2182A), PID temperature controller (Autonics TZN4S-14S), type-K thermocouple, and the sample was set up between the copper heater and a Teflon block on the cold side. By heating the copper block, the thermovoltage change (ΔV) as a function of the temperature difference (ΔT) between the contacts was recorded and the Seebeck coefficient (S) was calculated as $S = \Delta V/\Delta T$. Hall coefficient was measured at room temperature by an Ecopia HMS3000 Hall effect measurement system with a magnetic field of 0.51 T and an electric current of 1 mA with a good Ohm contact established using Au electrodes.

3 | RESULTS AND DISCUSSION

3.1 | Morphology, elemental, and structural analysis of doped rGO

The morphology of the GO sample which reveals the interconnected sheets of the GO structure are shown in

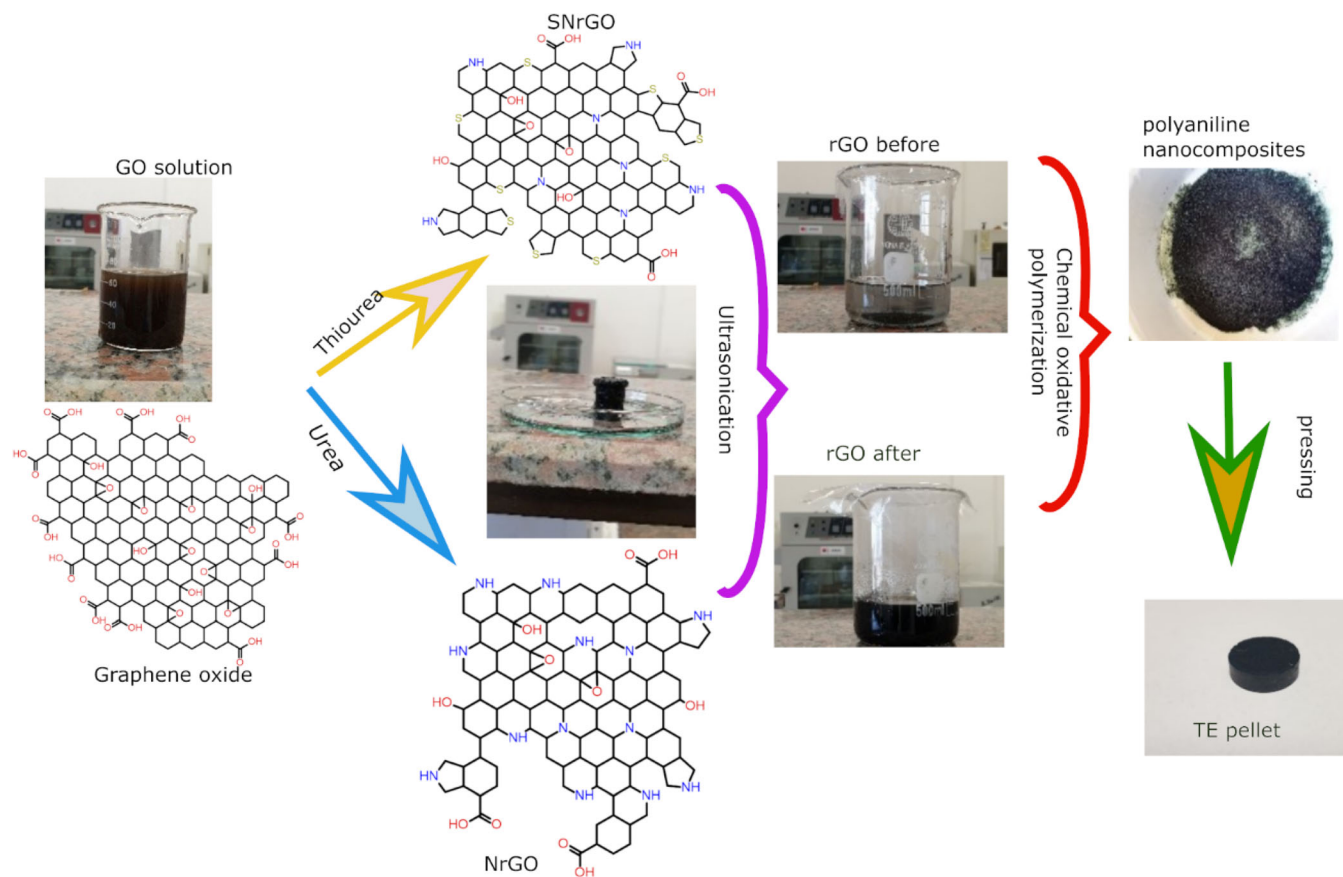
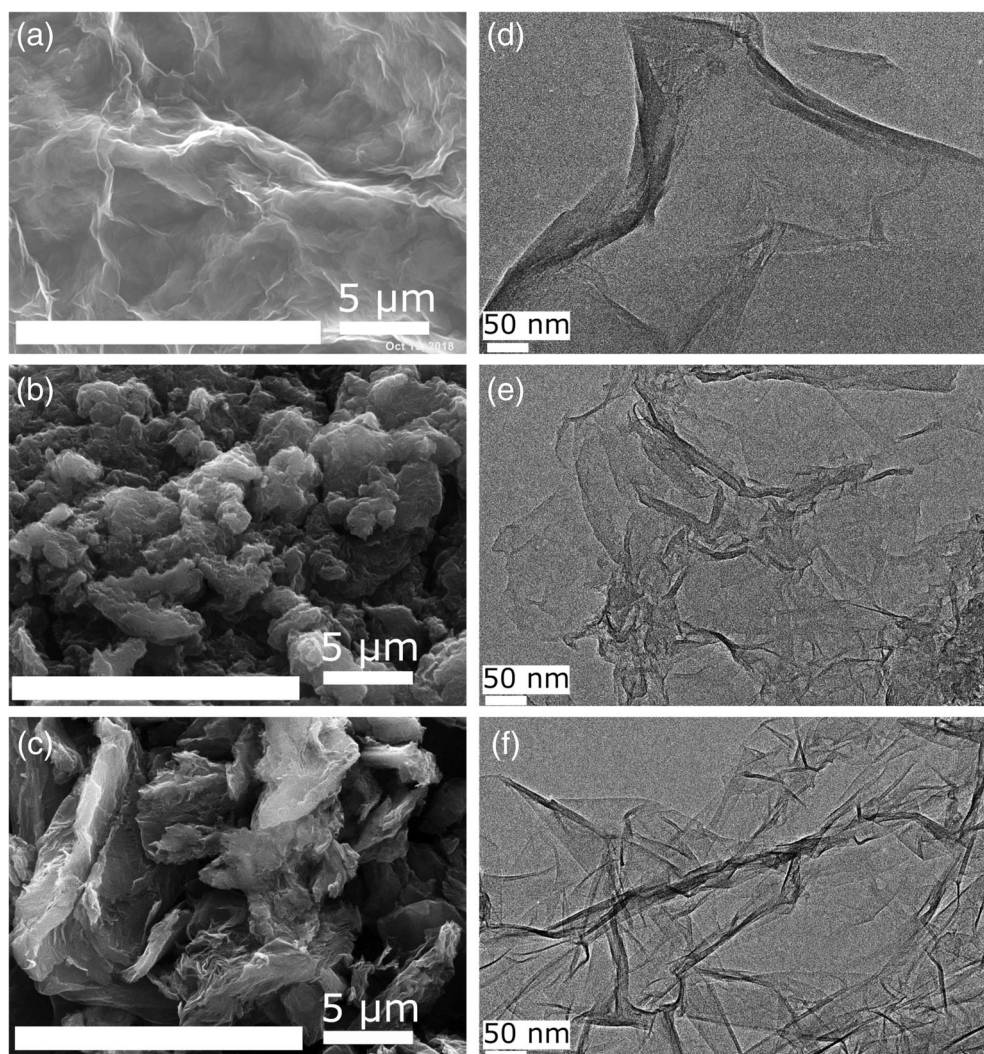


FIGURE 1 Schematic illustration of the preparation of doped reduced graphene oxide (rGO) and polyaniline nanocomposites [Color figure can be viewed at wileyonlinelibrary.com]

the SEM images in Figure 2(a) and TEM images in Figure 2(d). This typical morphology is attributed to the presence of tightly bound oxygen-functional groups (OFGs) on the GO. The oxygen groups impart GO with insulating properties and this is confirmed from the contrast variation of the GO morphology compared to the SEM micrographs in Figure 2(b),(c). The NrGO and SNrGO SEM images in Figure 2(b),(c) showed darker morphology which implies a higher conductivity owing to a restored sp^2 hybridization. A spongy morphology of NrGO consisting of small stacked rGO platelets was obtained, while the SEM image of SNrGO showed loosely packed structure and larger rGO flakes attributed to a better reducing effect of thiourea compared to that of urea. The combined effect of the ammonia and hydrogen sulfide in the thiourea makes it a strong reducing agent and better dopant compared to urea which only decomposes into ammonia during the hydrothermal process. Furthermore, the sulfur atoms introduced onto the graphene structure are larger in size than the nitrogen atoms thereby preventing restacking and hence the observed loose structure for the SN-doped sample compared to its N-doped counterparts. This is further

confirmed by the difference in the interplanar spacing from the XRD results of the NrGO and SNrGO samples. Additionally, from the TEM images of both samples shown in Figure 2(e) for NrGO and Figure 2(f) for SNrGO, large and more transparent SNrGO sheets were observed compared to NrGO which had higher wrinkle intensity because of its smaller sheets size. The fewer number of layers in SNrGO can also be attributed to the relatively larger size of the sulfur atoms than carbon and nitrogen atom that inhibit the restacking of the graphene sheets after drying. The much exfoliated SNrGO offers more exposed area which will facilitate effective PANI nucleation and polymerization and thus improved properties are envisioned. On the other side, the small NrGO sheets promote a higher number of boundary density which is essential for increasing the phonon scattering probabilities and hence a low thermal conductivity is anticipated.^{5,37} The elemental analysis and mapping of the NrGO sample, as a typical example of doped rGO, was studied via EDX and results are shown in Figure S3. The mapping images show a clear distribution of the signature elements; carbon, nitrogen and oxygen throughout the sample. The image for elemental carbon shows a

FIGURE 2 Scanning electron microscopy (SEM) micrographs of graphene oxide (GO) (a), nitrogen-doped rGO (NrGO) (b), and sulfur and nitrogen co-doped rGO (SNrGO) (c) and transmission electron microscopy (TEM) micrographs of GO (d), NrGO (e) and SNrGO (f)



homogenous distribution of carbon atoms because of their typical high packing density inside the structure. For nitrogen and oxygen related images, it is noticed that the atoms show very low packing density with random order or distribution due to their doping nature. The location of oxygen atoms refers to the remnants of unreduced OFGs. While the observed location of nitrogen atoms is mostly referred to the cured defect sites after the random removal of oxygen atoms in the form of C—O, O—C=O and C=O groups. We believe that the inclusion of nitrogen dopants in the structure of rGO sheets was beneficial for the restoration of the sp^2 domains of rGO sheets.

FTIR spectroscopy was used to analyze the chemical structure of the GO and heteroatom-doped rGO samples. In Figure 3(a), a typical FTIR spectrum of the prepared GO was obtained.^{38,39} After the hydrothermal process, the peak intensities of some of the OFGs in NrGO and SNrGO spectra were significantly reduced while other peaks were completely disappeared indicating the successful reduction of the graphene oxide and the restoration of sp^2 conductive domains in the rGO. The GO reduction is a resultant of the

reaction between the OFG and the highly reactive by-products from thiourea (ammonia and hydrogen sulfide) and urea (ammonia) in addition to the temperature and pressure within the hydrothermal vessel. Successful nitrogen doping was confirmed by the appearance of C—N, C=N, and C≡N absorption peaks in the NrGO spectrum,⁴⁰ while the presence of the SO_x^- and C—S—C absorption peaks in addition to the carbon-nitrogen peaks signified the S—N co-doping.^{35,41,42} A slight shift of the C=C bond in the SNrGO spectrum to 1685 cm^{-1} compared with 1640 cm^{-1} in the GO was observed, in addition to the relatively higher intensity of this bond in the SNrGO spectrum compared to that in the NrGO spectrum. This indicates that a higher distortion of sp^2 -hybridization due to squeezing by the larger sulfur atom in the graphene skeleton, and hence a better electrical performance is anticipated to be achieved for SNrGO-based nanocomposite.

The X-ray diffractograms of GO, NrGO and SNrGO are shown in Figure 3(b). The appearance of a sharp peak in the GO spectrum at $2\theta = 10.3^\circ$ associated with the (001) crystalline plane confirms the successful oxidation

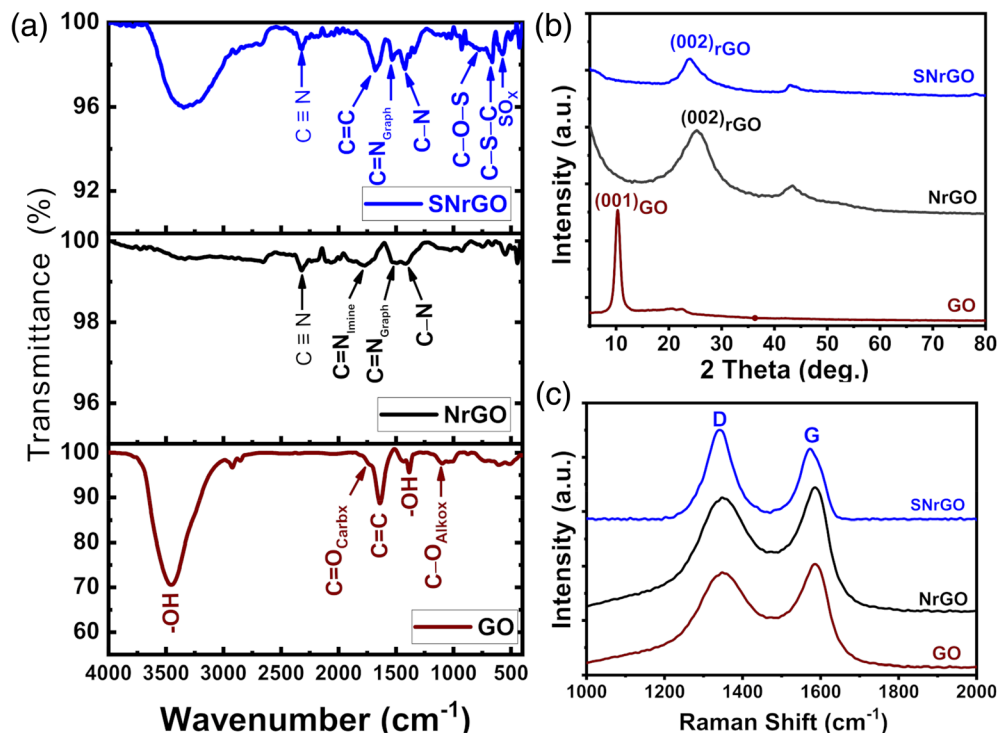


FIGURE 3 Fourier transform infrared (FTIR) spectra (a), X-ray powder diffractometer (XRD) patterns (b), Raman spectra (c) of graphene oxide (GO), nitrogen-doped rGO (NrGO), and sulfur and nitrogen co-doped rGO (SNrGO) [Color figure can be viewed at wileyonlinelibrary.com]

of graphite. This corresponds to an interplanar spacing (d) of 8.6 Å, which is greater than 3.36 Å for graphite owing to the intercalation of OFGs in between the graphitic layers of the graphite.^{40,41} Doping GO with urea/thiourea results in the disappearance of the diffraction peak at 10° suggesting the reduction of GO to NrGO and SNrGO respectively, which is in good agreement with our FTIR and also other studies.^{35,43} A broad 2θ peak related to (002) graphite crystalline plane is observed at 25.3 and 23.9° which corresponds to the interlayer distance of 3.5 and 3.7 Å for NrGO and SNrGO, respectively. The reduced interlayer distance from 8.6 Å to 3.5 and 3.7 Å also confirms the successful hydrothermal reduction process and retrieval of the sp^2 -hybridization of the graphene structure. Nevertheless, the broadening of this peak suggests that the NrGO and SNrGO have short-range order of carbon atoms.^{40,41} Moreover, the higher d value of the SNrGO is in good agreement with the TEM results discussed earlier which showed fewer number of layers and less restacking of the rGO.

Raman spectroscopy has been used widely to determine the defect density and disorder degree and crystallinity of carbon-based materials.^{44,45} The Raman spectra of GO, NrGO and SNrGO depicted in Figure 3(c) show the two main characteristic peaks correlated with graphene-based materials at approximately 1350 and 1585 cm^{-1} which correspond to D and G bands, respectively.⁴⁴ The ratio of the intensity of these bands (I_D/I_G) is majorly used to evaluate the quality of the prepared graphene.⁴⁵ From Table 1, the I_D/I_G are 0.92, 1.03 and

1.27 for GO, NrGO, and SNrGO respectively, which implies that heteroatom-doping resulted in structural defects in the graphitic structure of the rGO sheets.^{17,35,43} It was also observed that SN co-doping resulted in a much higher I_D/I_G ratio than NrGO which could be attributed to the large size of sulfur atoms compared to carbon atoms causing an additional induced strain in the graphitic structure.

The in-plane sp^2 crystallite size (L_a) for all graphene-based prepared materials was calculated according to Equation (2),⁴⁵ and the values represented in Table 1:

$$L_a(\text{nm}) = (2.4 \times 10^{-10}) \lambda^4 (I_D/I_G)^{-1} \quad (2)$$

where, λ is the Raman excitation wavelength, and I_D and I_G represent the relative intensity of D and G bands, respectively. The GO was seen to have the largest L_a of 20.9 nm and following the hydrothermal treatment and doping process, this value was decreased to 18.7 and 15.1 nm for NrGO and SNrGO respectively. This agrees with the study carried out by Rivera et al., in which they reported that the heteroatoms dopant broke the continuity of the sp^2 -framework and a subsequent reduction in the graphene crystallite size is obtained.⁴⁶

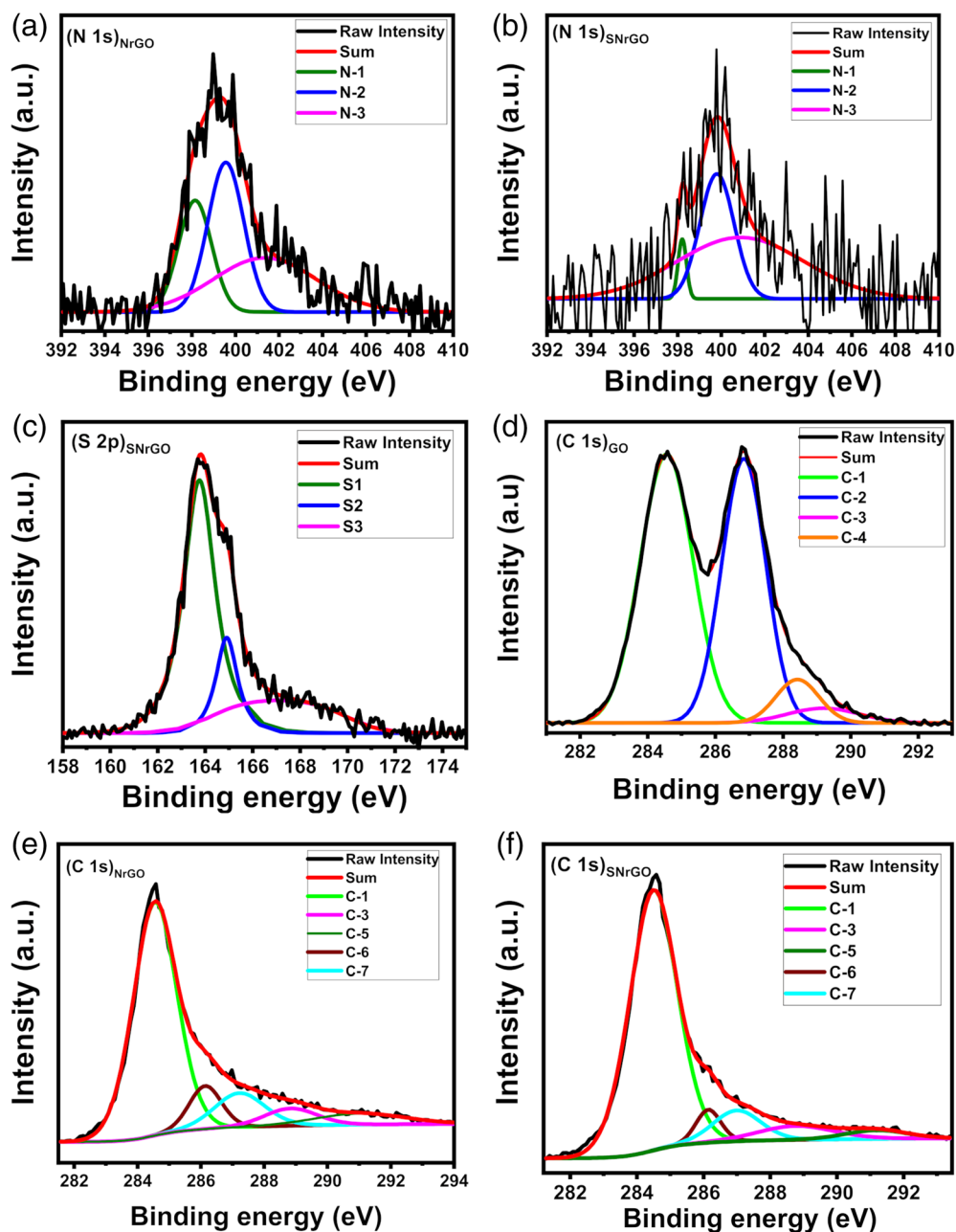
XPS measurement was done to further probe the chemical composition and the percentage of the elemental content of the GO and the doped rGO (Figure S1). The data was analyzed and the high-resolution XPS spectra represented in Figure 4 while the percentage elemental

TABLE 1 Summarized XRD, Raman, and XPS parameters for GO, NrGO, and SNrGO

Sample	Interplanar spacing (<i>d</i>) (nm)	I_D/I_G	L_a (nm)	C (At. %)	O (At. %)	N (At. %)	S (At. %)
GO	0.86	0.92	20.9	71.33	28.67	—	—
NrGO	0.35	1.03	18.7	79.02	12.50	8.48	—
SNrGO	0.37	1.27	15.1	85.02	9.56	3.80	1.62

Abbreviations: GO, graphene oxide; NrGO, nitrogen-doped rGO; SNrGO, sulfur and nitrogen co-doped rGO; XPS, X-ray photoelectron spectroscopy; XRD, X-ray powder diffractometer.

FIGURE 4 High-resolution X-ray photoelectron spectroscopy (XPS) N 1s spectra for nitrogen-doped rGO (NrGO) (a), N 1s spectra for sulfur and nitrogen co-doped rGO (SNrGO) (b), S 2p spectra for SNrGO (c), C 1s spectra for GO (d), C 1s spectra for NrGO (e), and C 1s spectra for SNrGO (f) [Color figure can be viewed at wileyonlinelibrary.com]



composition and doping degree was further summarized in Table 1. Figure 4(a) depicts the deconvoluted N 1s spectrum of NrGO and as observed three N-species, (N1-pyridinic [398.2 eV], N2-pyrrolic [399.6 eV], and

N3-graphitic [401.3 eV]) were present, which is in agreement with other nitrogen doping reports.^{41,43,47} A similar trend of the N-species was also reported in Figure 4(b) for the deconvoluted N 1s spectrum of the SNrGO however,

the relative amounts of each species varied from those in NrGO. The relative ratio of the N-species (N1, N2, and N3) was calculated based on the area of deconvoluted curves and reported as 25%, 37%, 38% for the NrGO and 4%, 34%, 62% for the SNrGO, respectively. The S 2p peak in the high-resolution XPS spectrum is shown in Figure 4(c) was resolved into two types of sulfur species. The higher binding energy of 167.1 eV was assigned to the oxidized-S which usually forms at the edges of the graphene. The second signal which split into peaks at 163.8 and 164.9 eV was attributed to thiophene-S (C—S—C) and the splitting peaks were assigned to S 2p_{3/2} and S 2p_{1/2}, respectively.^{31,38,39} The higher thiophene-S content could play an important role in the enhancement of the TE application via improving the charge carrier's mobility because it is mainly incorporated in the carbon framework.⁴⁸

The high-resolution C 1 s for GO in Figure 4(d) revealed the variation of carbon–oxygen configuration bonding with peaks observed at a binding energy of 284.8, 287.0, 288.5, 289.5 and 292 eV belonging to C—C, C—O, O—C=O and C=O respectively. It is worth noting that the high oxygen content of 28.67% in the GO structure was as a result of the high oxidation of the graphite and it was considerably reduced by more than half to 12.50% and 9.56% for the NrGO and SNrGO respectively after the hydrothermal-doping process as shown in Figure 4 (e),(f). This was accompanied by the relative increase in the carbon content from 71.3% for the GO to 79.0% for the NrGO and 85.0% for the SNrGO. This translates to a C/O ratio of 2.49, 6.32, and 8.89 for GO, NrGO, and SNrGO, respectively, which further confirms our earlier speculation about the superiority of the reducing efficiency of thiourea over urea. However, full reduction of the OFGs is still impossible at this low hydrothermal temperature as has been reported by some groups.^{35,42,47}

3.2 | Morphology, elemental, and structural analysis of PANI-rGO nanocomposites

The SEM images of the polyaniline and its nanocomposites are as shown in Figure S7, in the supplementary information. No significant changes were seen in the SEM images due to the low rGO amount hence further probing was conducted at higher magnification using the TEM. The TEM image of PANI-EB sample, Figure 5(a), reveals spherical shaped nanoparticles with clear necking and interconnection of PANI nanoparticles. The TEM images of the PANI/rGO nanocomposites on the other hand (Figure 5(b)–(e)) shows a uniform coating of doped rGO sheets with polyaniline nanoparticles. That is due to the strong electrostatic and π - π stacking interaction

between the rGO and the aromatic PANI structure arising mainly from the in situ polymerization and oxidation of aniline monomer directly on the rGO sheets. The strong interaction in the PANI/rGO is also presumed to significantly improve the chain alignment in the PANI and subsequently both the electrical and the thermal conductivities of the tailored nanocomposites. Noteworthy to mention that, increasing the percentage of SNrGO from 1 to 5 wt% led to a decrease in the amount of PANI nanoparticles attached to the individual SNrGO sheets (Figure 5(d),(e)) which is not observed in the NrGO case (Figure 5(b),(c)). This was mainly attributed to the larger expanded nature of the SNrGO discussed earlier, which enabled more exposed area for the polymerization of PANI, thereby resulting in a larger relative amount of PANI as opposed to NrGO. The elemental analysis and mapping images for PANI and its nanocomposites samples were also studied by EDX and the results are shown in Figures S4–S6 in the SI document. In brief, the images show good distribution of elemental carbon, nitrogen, oxygen, besides sulfur through-out the examined samples. This is an indication for the well dispersion, without agglomeration, of the doped rGO sheets throughout the structure of PANI.

The structural characteristics of the prepared PANI-EB and PANI/doped rGO nanocomposites were studied using the FTIR as shown in Figure 6(a). Characteristic peaks associated with PANI-EB were observed at approximately 1583 and 1498 cm^{−1} and these were attributed to the C=C stretching and the C—C stretching vibration mode in the quinoid ring and benzenoid rings, respectively.²⁰ This has been shown as proof of the presence of the amine and imine nitrogen units in the polyaniline backbone signifying successful preparation of emeraldine form of polyaniline which is conductive.^{20,36} The bands observed at 813 and 1128 cm^{−1} are assigned to the C—H out of plane deformation vibration modes for 1, 4 benzene ring and a stretching mode of B—NH⁺=Q which is formed during the acid doping process of polyaniline, respectively.^{20,36} The bands observed at 1298 and 1243 cm^{−1} were assigned to N—C—N stretching vibrations and C—N stretching. Following the in situ polymerization, additional minor peaks related to doped rGO were seen in the PNrGO and PSNrGO spectra. Nevertheless, the PANI peaks overshadowed the rGO peaks due to the minute amount of graphene sheet loadings in the nanocomposites.

The XRD patterns for PANI-EB and PANI/doped rGO nanocomposites are shown in Figure 6(b). The pattern of PANI-EB declares the characteristic diffraction peaks of polyaniline at 14.9, 20, and 25.1° which was indexed to (011), (020), and (200) planes, respectively. These peaks also reveal the semi-crystalline nature of the polymer

FIGURE 5 Transmission electron microscopy (TEM) images of polyaniline (PANI)-EB (a), PNrGO-1 (b) PNrGO-5 (c), PSNrGO-1 (d) and PSNrGO-5 (e)

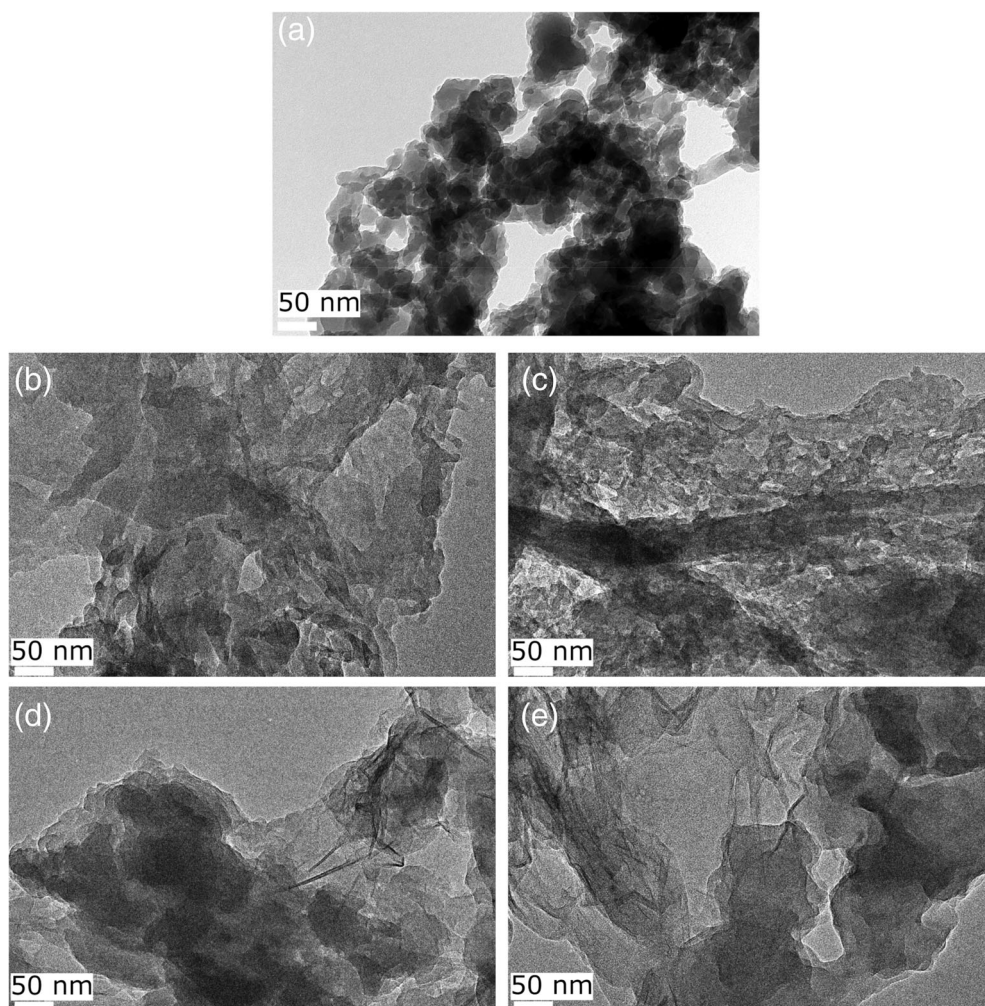
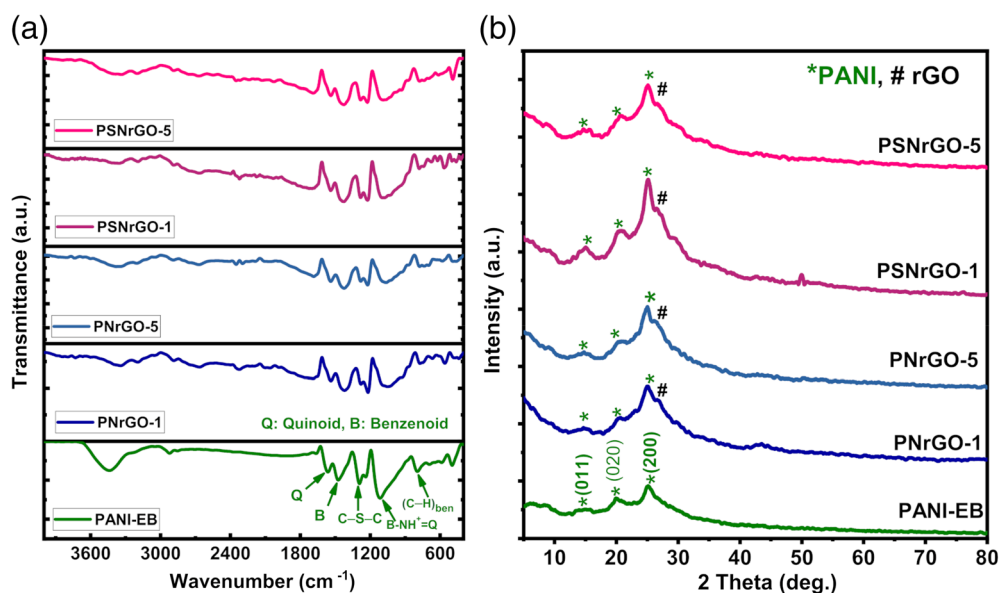


FIGURE 6 Fourier transform infrared (FTIR) (a), and X-ray powder diffractometer (XRD) (b) of polyaniline (PANI)-EB and PANI/doped rGO nanocomposites [Color figure can be viewed at wileyonlinelibrary.com]



arising from the rigid backbone due to the quinoid and benzenoid rings.²⁰ On the other hand, XRD measurements for PANI-rGO nanocomposites were able to detect

the presence of doped rGO via recording an extra shoulder peak at 26.5°, which is superimposed with the major peak, at 25.1°, typical of PANI structure. Additionally,

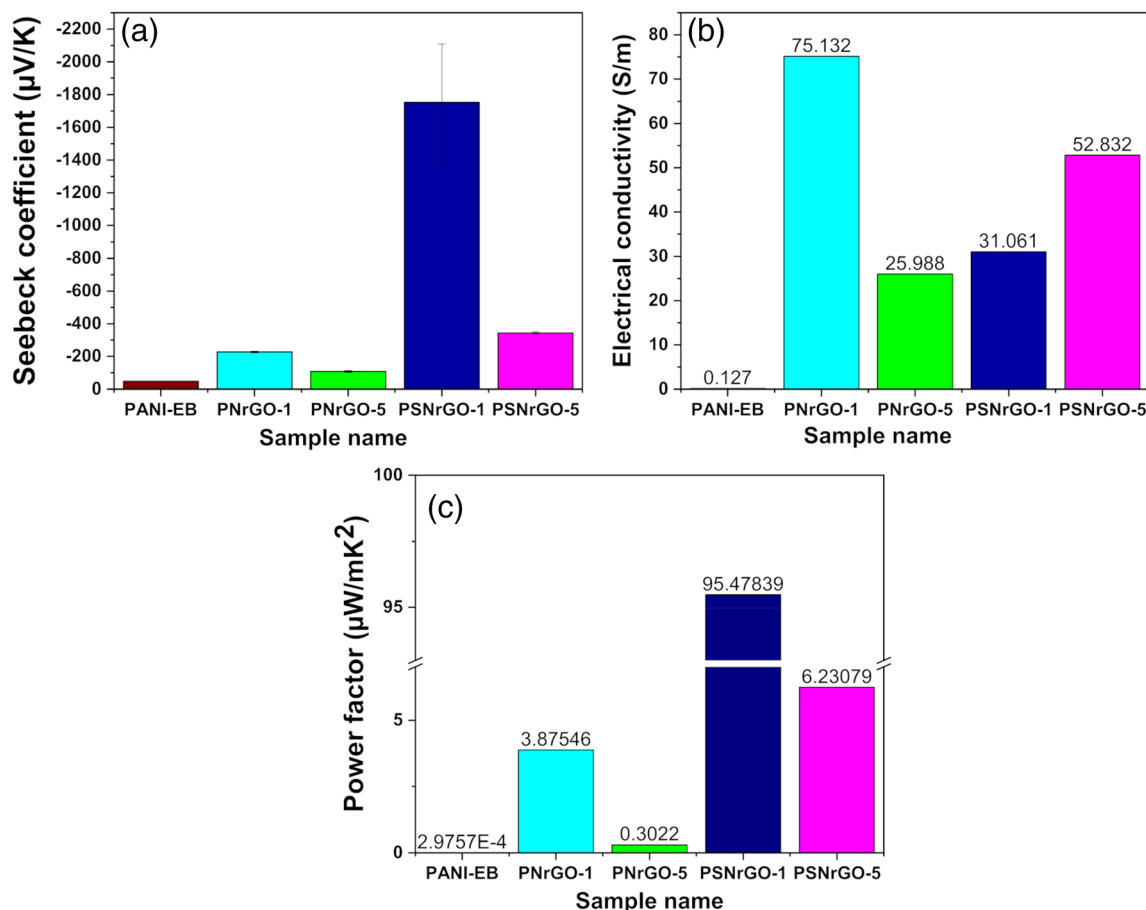


FIGURE 7 Composition dependent (a) Seebeck coefficient, (b) electrical conductivity, and (c) power factor of polyaniline and its nanocomposites [Color figure can be viewed at wileyonlinelibrary.com]

tapering of the PANI peak at 25.1° in the nanocomposites was also observed and this infers that there may be π - π stacking interaction between the rGO and the benzene rings in the polymer. These observations signify the successful integration of doped rGO sheets into the PANI structure.

3.3 | Thermoelectric properties of PANI-rGO nanocomposites

3.3.1 | Seebeck coefficient

The Seebeck coefficient (S) of all the prepared samples measured at room temperature is as shown in Figure 7(a). All samples demonstrated negative S values which are characteristic of n-type transport behavior. The n-type behavior in PANI and its nanocomposites is believed to originate from the ionic transport of the chloride ions through the PANI chains. In the presence of a temperature gradient and moisture-rich conditions, ionic Seebeck effect becomes a predominant conduction mechanism, and this

phenomenon is referred to as the Soret effect.^{30–32} This is responsible for generating the high thermal diffusion of the charge carriers giving rise to high S values, called ionic Seebeck coefficient.

The lowest S value equals -0.048 mV K^{-1} was reported for the plain PANI, which upon doping increased to 0.227 and -0.108 mV K^{-1} for PNRGO-1 and PNRGO-5, respectively. Generally, PSNRGO samples showed better improvement in the S value of the nanocomposite, with the highest S value of -1.75 mV K^{-1} being attained by the PSNRGO-1 sample. This was 36 times and 7 times more than PANI and PNRGO counterparts, respectively, and confirmed our earlier assumption on the superiority of the sulfur-nitrogen co-doped rGO as an additive for PANI. The addition of rGO into the PANI structure induces a templating effect during the polymerization process, leading to a more aligned and expanded conformation of the polymer chain structure compared to the coil-like PANI structure.^{19,20} The expanded conformation promotes the movement of chloride ions through the transport channels. Moreover, it also facilitates carrier hopping from one polymer chain to another resulting in

increased carrier mobility and this explains the noticeable enhancements in the S value of all synthesized nanocomposites. It is also believed that the higher S for the PSNrGO compared to PNrGO may have been influenced by the larger interplanar d spacing of the SNrGO over the NrGO.

We believe that the observed improvement in the Seebeck values agrees with the prediction from the Mott equation,⁵ whereby improved values are expected with a reduction in carrier concentration (n) and increase in carrier mobility (μ). Many studies have reported a strong π - π interaction between rGO and the aromatic PANI structure. Therefore, we anticipate that the energy level mismatch between PANI/rGO nano junction may cause the freezing of 'cold electrons' to allow only high energy electrons to pass. This energy filtering effect has been confirmed in many reports as a strategy for tuning S values for composite material.^{49,50} For PANI/rGO, a proposed energy filtering is demonstrated in Figure S2, and we consequently envision a decreased carrier concentration which is confirmed by the hall transport properties summarized in Table 2. The improved Seebeck values reported herein for the PANI and its nanocomposites are considerably higher compared to those reported for most other n-type PANI studies. These values are however still low in comparison to the reported S values as high as 18 mV K⁻¹ for PEDOT:PSS, which was at the expense of stability and high cost.³⁰⁻³²

3.3.2 | Electrical conductivity

From the electrical conductivity (σ) results in Figure 7(b), it was seen that pristine PANI attained a σ as low as 0.1 S m⁻¹ which is alleged to the highly disordered PANI structure. Transport characteristics of polyaniline are known to be disorder-dependent and this subsequently results in varied transport characteristics which fall in the metal-insulator range as described by many transport theories.⁵¹ The highly amorphous PANI structure hinders the effective passage of ions in the ion transport channels and the fast charge carrier transfer through hopping. Consequently, low carrier mobility is manifested resulting in low conductivity. However, upon adding doped rGO, the electrical conductivity is substantially increased to over one order of magnitude. PNrGO-1 reported the highest electrical conductivity of 75 S m⁻¹ which was 500 times higher compared with pristine PANI. However, a decreased conductivity was observed by increasing the rGO amount to 5 wt%. Conversely, for the PSNrGO nanocomposites, increasing the SN-rGO amount from 1 to 5 wt% led to enhanced electrical conductivity from 31 to 53 S m⁻¹.

TABLE 2 Summarized hall transport properties of PANI and PANI/rGO nanocomposites

Sample	Mobility (cm ² V ⁻¹ s ⁻¹)	Carrier concentration (10 ¹⁸ cm ⁻³)
PANI-EB	0.088	5.771
PNrGO-1	7.830	1.675
PNrGO-5	23.150	1.005
PSNrGO-1	56.350	0.657
PSNrGO-5	51.520	1.832

Abbreviations: PANI, polyaniline; rGO, reduced graphene oxide.

Many factors have been reported to contribute to the σ properties of heteroatom-doped rGO and PANI/rGO nanocomposites. The electronic properties of standalone heteroatom-doped rGO are influenced by factors such as the influence of the heteroatom on the Fermi level of the rGO, the bonding configuration of the heteroatoms, quality and packing of the graphene plates, amount of OFGs, carrier concentration among others.¹⁶⁻¹⁸ The Raman results showed a higher I_D/I_G for the SNrGO compared to the NrGO which indicates more defect level in the structure resulting from the large sulfur atoms. Reports have shown how the defect level of the rGO can impact the σ of graphene-based materials negatively. This fact implies that defect level played a major role in downplaying the fact that SNrGO contains a loose structure hence a lower conductivity was observed for its nanocomposites compared to PNrGO-1.

Furthermore, the XPS of the rGO samples showed a reduced amount of OFG in the rGO samples. Additionally, NrGO had a higher percentage of nitrogen than SNrGO and further deconvolution of the nitrogen XPS peak showed different in plane N-bonding configurations on the graphene sheet which is known to affect the electronic properties differently. We believe that the high nitrogen content in the NrGO resulted in a higher electrical conductivity in the PNrGO-1 compared to PSNrGO samples despite the starting material of the latter consisting of highly loose structure. For the PNrGO samples increasing this amount from 1 to 5 wt% does not improve the σ as expected despite the higher nitrogen content due to compact structure of the NrGO. A loose structure was beneficial when the SNrGO was increased from 1 to 5 wt% as portrayed in the increased σ in the PSNrGO, which evolved from an improved templating effect in the PANI chains which indicates a better energy filtering effect at the PANI/rGO nanojunctions.

It can thus be concluded that the conductivity in the polyaniline nanocomposite materials was influenced by the synergetic effect from the amount of heteroatom and

TABLE 3 Conductivity, Seebeck coefficient, and power factor for some reported polyaniline thermoelectric materials

Material	Seebeck coeff. ($\mu\text{V K}^{-1}$)	Electrical cond. (S m^{-1})	Thermal cond. ($\text{W m}^{-1} \text{K}^{-1}$)	Power factor ($\mu\text{W m}^{-1} \text{K}^{-2}$)	zT factor	Ref.
Polyaniline/S-N co-doped rGO (1 wt%)	-1.75×10^3	31.06	0.51	95.49	5.58×10^{-2}	This study
Polyaniline/S-N co-doped rGO (5 wt%)	-3.43×10^2	53.00	0.45	6.23	4.15×10^{-3}	This study
Polyaniline/ionic liquid	-1.39×10^2	2.30×10^{-1}	—	4.43×10^{-3}	—	26
Polyaniline/ H_2SO_4	-3.00	6.31×10^2	—	—	—	27
Polyaniline/DMSO/KH, NaH	—	1–10	—	—	—	28
Polyaniline/DWNT (8 wt%)	-12.00	0.11	—	—	—	29
Polyaniline/reduced graphene oxide (70 wt %)	-13.64	16.50	—	30.62	—	24
PANI/graphene nanoplate	19.00	1.74×10^4	15.00	—	1.26×10^{-4}	19
Polyaniline/reduced graphene oxide	32.64	1.81×10^3	0.14	2.00	4.60×10^{-3}	20
Polyaniline/graphene nanosheets	31.00	5.89×10^3	—	5.60	—	21
PANI-GO	59.00	1.49×10^5	—	5.21	—	22

bonding configuration in the rGO, the templating effect of the rGO sheets causing alignment of polymer chains, the energy filtering at the PANI/rGO nano junctions, and so on.

Despite the conductivity improvements obtained here, the values are still low compared to previously reported values for p-type PANI-based materials.^{19–23} This is because the transport behavior is strongly dominated by the ionic conduction, hence the control of charge carrier concentration and optimizing ionic transport characteristics for n-type materials are still major concerns among researchers.^{25,26,30} Nonetheless, our findings are interesting in that the remarkable enhancements achieved are with the usage of very small amounts of modified rGO superior to other previous studies that used up to 70 wt% loadings to achieve satisfying enhancements.^{12,23,24}

3.3.3 | Power factor

The calculated PF of the PANI and its nanocomposites are presented in Figure 7(c). The PF for the pristine polymer was the lowest at $3 \times 10^{-4} \mu\text{W m}^{-1} \text{K}^{-2}$, with the addition of rGO, the values were substantially increased because of the simultaneously increasing S and σ . The PF for the PNrGO-1 and PSNrGO-1 are 4 and $96 \mu\text{W m}^{-1} \text{K}^{-2}$, respectively, nearly four orders of magnitude higher than the pristine PANI. Regardless of the relatively low ionic conductivity of the PSNrGO-1 than PNrGO-1, the dramatic increase in its S along with the square dependence of the PF on the Seebeck coefficient

led to the high attained PF value. It is worthy to mention that the PF values reported here are among the highest reported PF for n-type PANI. For comparison purposes, the TE characteristics including those of some p-type materials have been profiled in Table 3.

3.3.4 | Thermal conductivity and figure of merit

PANI is a desirable candidate for TE application due to its low thermal conductivity arising from its semi-crystalline nature and highly disordered structure which heavily suppresses the localized thermal transport. Figure 8(a) shows the room temperature thermal conductivity (κ) for the measured samples. As can be seen, the recorded κ for the pristine PANI is $0.29 \text{ W m}^{-1} \text{K}^{-1}$. Upon the addition of different amounts from the rGO, the κ is increased to 0.38, 0.40, 0.51, and $0.45 \text{ W m}^{-1} \text{K}^{-1}$ for PNrGO-1, PNrGO-5, PSNrGO-1, and PSNrGO-5 respectively. All the measured values are still below $1 \text{ W m}^{-1} \text{K}^{-1}$, which agrees well with previous reports on PANI/carbon-based nanocomposites.^{19,20} This likely small increase in the κ of the PANI after compositing with the rGO may be attributed to phonon scattering effect by the wrinkles of the rGO sheets and at the PANI/rGO nanointerfaces which suppress phonon transport.^{5,37}

This contributes favorably to the room temperature figure of merit (zT) calculated for the samples as shown in Figure 8(b). All the PANI/rGO nanocomposites showed an improved zT factor compared to pristine PANI

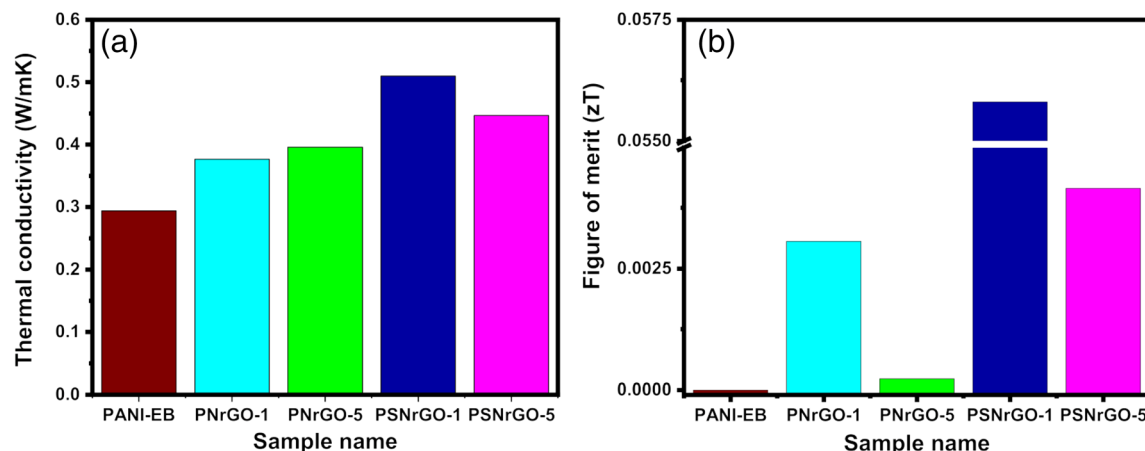


FIGURE 8 Composition dependent (a) thermal conductivity, and (b) figure of merit of polyaniline and its nanocomposites [Color figure can be viewed at [wileyonlinelibrary.com](https://onlinelibrary.wiley.com)]

and the best value was estimated to be 5.6×10^{-2} for PSNrGO-1, that is five orders of magnitude higher than the 3.02×10^{-7} for pristine PANI. Several PANI/graphene studies reported enhanced zT values in the range of 10^{-2} – 10^{-6} ,^{19,20,23} however, most of them focused on p-type materials which were achieved with higher amounts of graphene loading. In this study with as low as 1 wt% rGO, the zT factor could be enhanced from a combined effect of the doping, energy filtering and so on discussed earlier.

4 | CONCLUSION

In summary, nanocomposites from PANI and doped rGO with n-type conductivity characteristics for thermoelectric applications were successfully prepared. The NrGO and SNrGO were first synthesized from GO through a facile hydrothermal technique. Whereas the polyaniline/doped-rGO nanocomposites were prepared via the in situ chemical oxidative polymerization of aniline in the presence of different amounts of rGO. Structural analysis such as FTIR, XPS, Raman spectroscopy ascertained the successful doping and reduction of the GO as well as the integration between the PANI nanoparticles and the rGO. A simultaneous improvement in the electrical conductivity and Seebeck coefficient of the PANI upon adding the rGO was observed. A Seebeck coefficient of -1.75 mV K^{-1} and a reasonable electrical conductivity of 31 S m^{-1} and low thermal conductivity of $0.51 \text{ W m}^{-1} \text{ K}^{-1}$ were recorded for the nanocomposites containing only 1 wt% of the SNrGO. This led to an optimized power factor of $95 \mu\text{W m}^{-1} \text{ K}^{-2}$ and a room temperature figure of merit of 0.05. These findings suggest that co-doped rGO is promising for tuning the TE properties of

polyaniline which may contribute to advancing the search for n-type TE organic materials.

ACKNOWLEDGMENT

The authors would like to acknowledge the Japan International Corporation Agency (JICA) and Egypt-Japan University for Science and Technology (EJUST) for supporting this work. This research was also conducted as part of the research project: graphene center of excellence for energy and electronic applications (ID 31306) that is supported by science and technology development fund (STDF) in Egypt.

ORCID

Mariam Kassim Ali <https://orcid.org/0000-0002-4592-8617>

Amr Hessein <https://orcid.org/0000-0002-7946-3053>

Mohsen A. Hassan <https://orcid.org/0000-0001-8599-7732>

Mohsen Ghali <https://orcid.org/0000-0001-9368-1172>

Ahmed Abd El-Moneim <https://orcid.org/0000-0002-9512-7201>

REFERENCES

- [1] D. Rowe, *Renew. Energy* **1994**, 5, 1470.
- [2] K. Hashimoto, A. A. El-Moneim, N. Kumagai, K. Asami, *ECS Trans.* **2006**, 1, 491.
- [3] A. Hussain, S. M. Arif, M. Aslam, *Renew. Sustainable Energy Rev.* **2017**, 71, 12.
- [4] M. N. Hasan, H. Wahid, N. Nayan, M. S. Mohamed Ali, *Int. J. Energy Res.* **2020**, 44, 6170.
- [5] L. Yang, Z. G. Chen, M. S. Dargusch, J. Zou, *Adv. Energy Mater.* **2018**, 8, 1701797.
- [6] C.-J. Yao, H.-L. Zhang, Q. Zhang, *Polymer* **2019**, 11, 107.
- [7] G. Chen, W. Xu, D. Zhu, *J. Mater. Chem. C* **2017**, 5, 4350.

- [8] Z. Soleimani, S. Zoras, B. Ceranic, S. Shahzad, Y. Cui, *Sustainable Energy Technol. Assessments* **2020**, 37, 100604.
- [9] P. Singh, S. Shukla, *J. Mater. Sci.* **2020**, 55, 1331.
- [10] G. Ćirić-Marjanović, *Synth. Met.* **2013**, 177, 1.
- [11] M. Bharti, A. Singh, S. Samanta, D. Aswal, *Prog. Mater. Sci.* **2017**, 93, 270.
- [12] W. Wang, Q. Zhang, J. Li, X. Liu, L. Wang, J. Zhu, W. Luo, W. Jiang, *RSC Adv.* **2015**, 5, 8988.
- [13] K. S. Novoselov, V. Fal, L. Colombo, P. Gellert, M. Schwab, K. Kim, *Nature* **2012**, 490, 192.
- [14] J. Zhao, D. Tan, G. Chen, *J. Mater. Chem. C* **2017**, 5, 47.
- [15] M. Gamil, O. Tabata, K. Nakamura, A. M. R. El-Bab, A. A. El-Moneim, *Sensor Rev.* **2016**, 36, 140.
- [16] W. Yu, L. Sisi, Y. Haiyan, L. Jie, *RSC Adv.* **2020**, 10, 15328.
- [17] H. Liu, Y. Liu, D. Zhu, *J. Mater. Chem.* **2011**, 21, 3335.
- [18] C. Hu, D. Liu, Y. Xiao, L. Dai, *Prog. Nat. Sci.: Mater. Int.* **2018**, 28, 121.
- [19] J. Xiang, L. T. Drzal, *Polymer* **2012**, 53, 4202.
- [20] M. Mitra, C. Kulsi, K. Chatterjee, K. Kargupta, S. Ganguly, D. Banerjee, S. Goswami, *RSC Adv.* **2015**, 5, 31039.
- [21] Y. Du, S. Z. Shen, W. Yang, R. Donelson, K. Cai, P. S. Casey, *Synth. Met.* **2012**, 161, 2688.
- [22] V. Shalini, M. Navaneethan, S. Harish, J. Archana, S. Ponnusamy, H. Ikeda, Y. Hayakawa, *Appl. Surf. Sci.* **2019**, 493, 1350.
- [23] Y. Zhao, G.-S. Tang, Z.-Z. Yu, J.-S. Qi, *Carbon* **2012**, 50, 3064.
- [24] M. K. Ali, A. A. Moneim, *Key Eng. Mater.* **2020**, 835, 200.
- [25] Y. Lu, J.-Y. Wang, J. Pei, *Chem. Mater.* **2019**, 31, 6412.
- [26] D. Yoo, J. J. Lee, C. Park, H. H. Choi, J.-H. Kim, *RSC Adv.* **2016**, 6, 37130.
- [27] C. Yoon, M. Reghu, D. Moses, A. Heeger, Y. Cao, T.-A. Chen, X. Wu, R. Rieke, *Synth. Met.* **1995**, 75, 229.
- [28] M.-Y. Hua, G.-W. Hwang, Y.-H. Chuang, S.-A. Chen, R.-Y. Tsai, *Macromolecules* **2000**, 33, 6235.
- [29] F. Yakuphanoglu, B. F. Şenkal, *Polym. Adv. Technol.* **2008**, 19, 905.
- [30] B. Kim, J. U. Hwang, E. Kim, *Energy Environ. Sci.* **2020**, 13, 859.
- [31] G.-H. Kim, J. Kim, K. P. Pipe, *Appl. Phys. Lett.* **2016**, 108, 093301.
- [32] H. Wang, U. Ail, R. Gabrielsson, M. Berggren, X. Crispin, *Adv. Energy Mater.* **2015**, 5, 1500044.
- [33] W. S. Hummers Jr., R. E. Offeman, *J. Am. Chem. Soc.* **1958**, 80, 1339.
- [34] M. Hirata, T. Gotou, S. Horiuchi, M. Fujiwara, M. Ohba, *Carbon* **2004**, 42, 2929.
- [35] X. Ren, J. Feng, P. Si, L. Zhang, J. Lou, L. Ci, *Chemosphere* **2018**, 210, 120.
- [36] E. Gomes, M. Oliveira, *Am. J. Polym. Sci.* **2012**, 2, 5.
- [37] K. Biswas, J. He, I. D. Blum, C.-I. Wu, T. P. Hogan, D. N. Seidman, V. P. Dravid, M. G. Kanatzidis, *Nature* **2012**, 489, 414.
- [38] A. Hessein, A. A. El-Moneim, World Congress on New Technologies(NewTech 2021) **2015**, 307.
- [39] S. Sayed, M. Gamil, A. F. El-Bab, K. Nakamura, T. Tsuchiya, O. Tabata, A. A. El-Moneim, *Sensor Rev.* **2016**, 36, 140.
- [40] L. Sun, L. Wang, C. Tian, T. Tan, Y. Xie, K. Shi, M. Li, H. Fu, *RSC Adv.* **2012**, 2, 4498.
- [41] T. Wang, L.-X. Wang, D.-L. Wu, W. Xia, D.-Z. Jia, *Sci. Rep.* **2015**, 5, 9591.
- [42] Y. Su, Y. Zhang, X. Zhuang, S. Li, D. Wu, F. Zhang, X. Feng, *Carbon* **2013**, 62, 296.
- [43] Z. Ramezani, H. Dehghani, *Int. J. Hydrogen Energy* **2019**, 44, 13613.
- [44] Z. Zafar, Z. H. Ni, X. Wu, Z. X. Shi, H. Y. Nan, J. Bai, L. T. Sun, *Carbon* **2013**, 61, 57.
- [45] L. Cançado, K. Takai, T. Enoki, M. Endo, Y. Kim, H. Mizusaki, A. Jorio, L. Coelho, R. Magalhaes-Paniago, M. Pimenta, *Appl. Phys. Lett.* **2006**, 88, 163106.
- [46] L. M. Rivera, S. Fajardo, M. D. C. Arévalo, G. García, E. Pastor, *Catalysts* **2017**, 7, 278.
- [47] T. Van Khai, H. G. Na, D. S. Kwak, Y. J. Kwon, H. Ham, K. B. Shim, H. W. Kim, *J. Mater. Chem.* **2012**, 22, 17992.
- [48] Z. Liu, H. Nie, Z. Yang, J. Zhang, Z. Jin, Y. Lu, Z. Xiao, S. Huang, *Nanoscale* **2013**, 5, 3283.
- [49] C. Meng, C. Liu, S. Fan, *Adv. Mater.* **2010**, 22, 535.
- [50] C. Gayner, Y. Amouyal, *Adv. Funct. Mater.* **2019**, 30, 1901789.
- [51] M. N. Gueye, A. Carella, J. Faure-Vincent, R. Demadrille, J.-P. Simonato, *Prog. Mater. Sci.* **2019**, 108, 100616.

SUPPORTING INFORMATION

Additional supporting information may be found online in the Supporting Information section at the end of this article.

How to cite this article: Ali MK, Hessein A, Hassan MA, et al. Heteroatom-doped reduced graphene oxide/polyaniline nanocomposites with improved n-type thermoelectric performance. *J Appl Polym Sci.* 2021;138:e50852. <https://doi.org/10.1002/app.50852>